ISSN 1063-7826, Semiconductors, 2011, Vol. 45, No. 6, pp. 798–804. © Pleiades Publishing, Ltd., 2011.
Original Russian Text © O.Ya. Olikh, 2011, published in Fizika i Tekhnika Poluprovodnikov, 2011, Vol. 45, No. 6, pp. 816–822.

PHYSICS OF SEMICONDUCTOR DEVICES

Features of Dynamic Acoustically Induced Modification of Photovoltaic Parameters of Silicon Solar Cells

O. Ya. Olikh

Taras Shevchenko National University of Kyiv, ul. Volodymyrska 62, 01601 Kyiv, Ukraine
e-mail: olikh@univ.kiev.ua

Submitted November 11, 2010; accepted for publication November 23, 2010

Abstract—The results of an experimental study of silicon solar cells operating under conditions of dynamic ultrasonic loading are presented. Based on an analysis of current–voltage characteristics, the dependences of the short-circuit current, open-circuit voltage, maximum output power, shunt resistance, reverse current, and breakdown voltage on the strain caused by acoustic waves of various frequencies are studied. Possible mechanisms of the acoustic effect are analyzed. In particular, acoustically induced transformation of recombination centers (e.g., B_SO_{2i} complexes) and ionization of levels associated with extended defects in the p–n junction region are considered.

DOI: 10.1134/S1063782611060170

1. INTRODUCTION

As is known, one of the ways to improve the operating characteristics of semiconductor structures and devices is modification of their defect subsystem, so-called defect engineering. Undoubtedly, the most commonly used methods to achieve these objectives are irradiation and heat treatment. However, these methods are not free of disadvantages, which is stimulating interest in the study of alternative ways to control defects. In particular, recently, rather broad interest has been paid to the use of ultrasonic (ultrasound) waves for such purposes [1]. For example, the ultrasound effects on the defect subsystem of semiconductor materials (defect rearrangement [2, 3], low-temperature annealing of radiation defects [4], ordering of complexes and nanoclusters [3, 5]), and acoustically induced (AI) changes in general properties of semiconductor barrier structures [6, 8] were detected. However, the collected experimental results are insufficient for technological applications of ultrasound and complete understanding of the physics of all processes in semiconductors during acoustic wave propagation. Furthermore, the vast majority of studies are devoted to irreversible residual effects of acoustic perturbations. At the same time, the effects occurring only during ultrasonic loading (USL) and disappearing after its termination remain poorly understood, but interesting [9]. Meanwhile, exactly such dynamic phenomena can be used to develop a new class of acoustically controlled semiconductor devices.

The objective of this research is the experimental study of features of operation of silicon solar cells (SCs) under USL conditions and the determination of mechanisms of the acoustic effect on photoelectric characteristics of Si structures with p–n junctions. On the one hand, the choice of such structures was dictated by their wide applications in various fields; on the other hand, this choice was determined by the good state of previous studies of them, which, in turn, made it possible to narrow the range of possible mechanisms of the sound–defect interaction.

2. EXPERIMENTAL

The structures to be studied consisted of a Czochralski-grown substrate (Cz-p-Si) doped with boron ($p = 1.25 \times 10^{15}$ cm^{-3}), of thickness $d_p = 300$ μm, on which an n-type ($n \approx 10^{19}$ cm^{-3}) layer of thickness $d_n \approx 0.5$ μm was obtained by phosphorus ion implantation. Aluminum contacts were fabricated on SC surfaces: one continuous contact on the p-region and a contact grid on the n-region. The sample area was $S_s \approx 1$ cm^2.

Current–voltage (I–V) characteristics of SCs were measured under various conditions. To this end, a setup based on an ADA-1282 analog-to-digital converter was used. It allowed measurements of forward and reverse I–V portions in the dc current range from 3×10^{-10} to 10^{-3} A with voltage step $V = 0.01$ V. Measurements were performed under the following conditions.

(i) The sample temperature was varied in the range of 290–330 K.

(ii) The sample was in darkness or its n-layer side was exposed to monochromatic light (with wavelength $\lambda = 900$ or 600 nm). The choice of monochromatic light with these wavelengths λ was dictated by the purpose of localizing the carrier photogeneration region; i.e., at $\lambda = 600$ nm, the effective depth of light absorption by silicon is $d_\lambda \approx 2$ μm, which is comparable to both d_n and the p–n junction width d_{pn} (~0.9 μm).

Hence, photogeneration will occur in the n-type layer, in the region of the p–n junction itself, and in the diode base. At the same time, $d_\lambda \approx 25$ μm at $\lambda = 900$ nm; in this case, only carrier generation deep in the p-type region, far from the space-charge region, can be considered.

(iii) For acoustically loaded samples, replaceable piezoelectric transducers were used, which allowed sequential excitation longitudinal waves with frequencies $f_{us} = 4.1$, 8.0, and 26.1 MHz. The USL technique is described in [10]. Since irreversible changes can occur in the silicon defect subsystem at the USL intensity $W_{us} > 1$ W/cm^2 [3, 4], waves with $W_{us} < 0.8$ W/cm^2 were excited in the case at hand, which corresponds to the relative strain in the ultrasonic wave

$$\varepsilon_{us} = \sqrt{2W_{us}/\rho_{Si}v_{us}^3} < 3.5 \times 10^{-6},$$

where ρ_{Si} is the silicon density and v_{us} is the speed of sound.

The measured forward portion of the I–V characteristic of the sample in dark was approximated by the standard formula [11]

$$I = I_0\left[\exp\left(\frac{qV}{E_T}\right) - 1\right] + \frac{V}{R_{sh}}, \quad (1)$$

where I_0 is the saturation current, E_T is the characteristic energy, R_{sh} is the shunt resistance, and q is the elementary charge. The least-squares approximation using statistical weight factors allowed us to determine I_0, E_T, and R_{sh}. The I–V characteristic measured upon exposure to light by the standard technique [11] was used to determine the open-circuit voltage V_{oc}, short-circuit current I_{sc}, and the maximum output power P_M. In this case, the I–V characteristic itself is described by the expression

$$I = I_0\left[\exp\left(\frac{qV}{E_T}\right) - 1\right] + \frac{V}{R_{sh}} - I_{sc}. \quad (1a)$$

As a parameter characterizing SCs under reverse bias, the reverse current at $|V| = 2\text{ V} - I_{R,2\text{ V}}$ was used. Furthermore, the analysis of the I–V characteristic allowed the determination of the breakdown voltage V_b. The values of these parameters in the absence of USL are listed in the table.

The objective of this research is to study the effect of sign-alternating deformation on the semiconductor structure parameters; therefore, it was necessary (a) to exclude the piezoelectric field penetration into the sample (this was provided by shielding the piezoelectric element [10]) and (b) to separate the effects of ultrasound and heating accompanying USL.

To satisfy item (b), a special measuring and data processing procedure was used, consisting of the following sequence of steps.

Solar cell parameters without ultrasonic loading

Parameter	Illumination wavelength λ, nm	Temperature, K	
		290	320
V_{oc}, V	900	0.275	0.193
	600	0.130	0.059
I_{sc}, 10^{-5} A	900	16.0	18.5
	600	1.87	1.82
P_m, 10^{-6} W	900	21.4	15.8
	600	0.82	0.31
E_T, eV	Absent	0.070	0.070
I_0, 10^{-6} A	″	2.1	8.2
R_{sh}, 10^4 Ω	″	2.3	1.3
V_b, V	″	4.7	4.8
$I_{R,2\text{ V}}$, 10^{-4} A	″	1.2	1.8

(i) An I–V characteristic was measured in the range of 290–330 K with a step of 1.5 K, and the temperature dependence of parameter P (P is V_{oc}, I_{sc}, P_M, I_0, E_T, R_{sh}, $I_{R,2\text{ V}}$, V_b) was determined under conditions of sound-free heating of the sample, $P = f(T)$.

(ii) During USL, for each value of $\varepsilon_{us}(W_{us})$, under conditions of steady-state temperature (~40 min after the USL onset), the desired parameter P^{us} was determined and the sample temperature T^{us} was measured. Experiments showed that AI heating did not exceed 20°C at maximum ε_{us}.

(iii) Using the determined dependences $P = f(T)$ and the values of T^{us}, the parameter P^T corresponding to a given temperature without USL was calculated ($P^T = f(T^{us})$).

(iv) As a quantitative indicator of the ultrasound effect, absolute $\Delta P = P^{us} - P^T$ or relative $\varepsilon P = (P^{us} - P^T)/P^T$ changes in the parameters, which account for corrections to heating, were considered; i.e., the additive property of temperature and AI changes in the SC parameters was admitted, which is allowed by the small temperature variation range during USL.

(v) To verify the reversibility of AI changes and the admissibility of the accepted procedure after USL termination, the sample was repeatedly heated to T^{us} and the parameter $P^{T/}$ was measured. As the experiments presented in Sections 3 and 5 showed, the results are almost identical ($P^T \approx P^{T/}$).

3. MAIN RESULTS AND DISCUSION

3.1. Charge Transport Mechanism

It is clear that a rigorous analysis of the effect of external factors (in particular, ultrasound) on current flow parameters can be performed only based on

charge transport mechanisms in a given structure. The study of the temperature dependences of I–V characteristics in the absence of USL allowed us to determine these mechanisms. For example, it was experimentally found that E_T is almost independent of temperature in the temperature range under study (E_T = (0.070 ± 0.003) eV), whereas I_0 exponentially increases,

$$I_0 = I_{00}\exp(\chi T), \quad (2)$$

where I_{00} and χ are constants also independent of SC temperature, $I_{00} = (1.8 \pm 0.1) \times 10^{-12}$ A, $\chi \approx 0.048$ K^{-1}.

Such temperature dependences of I_0 and E_T are indicative of the tunneling current mechanism [11, 12] in the studied structures. This conclusion correlates with the results of [13], where it is shown that carrier tunneling is dominant during charge transport in many nanodisordered materials, including ion-doped ones.

In [12], it was assumed that tunneling in p–n structures can result from the carrier transition over an extensive chain of deep levels in the space-charge region caused by structural defects. In this case, I_{00} is defined by the deep-level concentration and E_T characterizes the defect type and is defined by such a phenomenological parameter as the curvature r_b of the parabolic barrier between localized centers,

$$E_T = \frac{\hbar}{\pi}\sqrt{\frac{r_b}{m^*}}, \quad (3)$$

where m^* is the electron effective mass. In this case, the distance δ_d between local levels can be estimated as the barrier width,

$$\delta_d = 2\sqrt{\frac{E_{b,\max}}{r_b}}, \quad (4)$$

where $E_{b,\max}$ is the barrier height. Assuming that $E_{b,\max} = qU_k/2$ (U_k is the contact potential difference) at zero bias, similar calculations in the case at hand show that $r_b = 0.11$ J/m^2 and $\delta_d = 1.6$ nm. We note that the latter value is quite realistic and corresponds to the distance of several lattice parameters.

If the defects causing the deep levels and facilitating tunneling are dislocations, then [12]

$$I_0 = q\rho_d\nu_D S_s \exp\left(-\frac{qU_k}{E_T}\right), \quad (5)$$

where ρ_d is a certain effective density of dislocations involved in tunneling and ν_D is the Debye frequency. The calculations according to (5) using the values $\nu_D = 1.35 \times 10^{13}$ s^{-1} and $I_0 = 2.1 \times 10^{-6}$ A showed that $\rho_d \approx 1.5 \times 10^5$ cm^{-2} at $T = 290$ K.

Within the above theory of tunneling over a chain of local levels [12], the quantity χ depends on the majority carrier concentration in p- and n-type regions,

$$\chi = \frac{\beta + kT\ln(N_c N_v n^{-1} p^{-1})}{E_T}, \quad (6)$$

where β is the temperature coefficient of band-gap narrowing, $E_g(T) = E_g(0) - \beta T$ (for Si, $\beta = 4.1 \times 10^{-4}$ eV/K), and N_c and N_v are the effective densities of states near the bottom of the conduction band and the top of the valence band, respectively. The value $\chi \approx 0.020$ K^{-1} calculated by formula (6) is close to 0.048 K^{-1} obtained by analyzing the experimental data according to (2), which indirectly confirms the applicability of this theory to the case at hand.

The reverse portion at $|V| < 4$ V is described by the power-law dependence

$$I \propto V^m, \quad (7)$$

where the coefficient $m \approx 1.1$. This suggests that the space-charge-limited current flows under velocity saturation condition in this case and the number of injected carriers is smaller than the number of thermally activated carriers [14].

Experiments showed that the SC resistance R_R under reverse bias is described by the expression

$$R_R^{-1} = R_{R,\mathrm{sh}}^{-1} + R_{R,p-n}^{-1}, \quad (8)$$

where $R_{R,\mathrm{sh}}$ is the temperature-independent quantity, $R_{R,\mathrm{sh}} \approx 2.0 \times 10^4$ Ω, and $R_{R,p-n}$ has a thermally activated nature ($R_{R,p-n} \propto \exp(E_{R,\mathrm{act}}/kT)$; $R_{R,p-n} \approx 2.2 \times 10^6$ Ω at $T = 290$K. Quite expected expression (8) shows that the SC equivalent circuit consists of two parallel resistances, one of which is associated with shunting processes and the other of which is directly associated with the depletion region. The quantity $R_{R,\mathrm{sh}} \sim 2.0 \times 10^4$ Ω is close to $R_{\mathrm{sh}} \sim 2.3 \times 10^4$ Ω obtained by approximating the forward portion of the I–V characteristic. The disagreement between $R_{R,\mathrm{sh}}$ and R_{sh} confirms the known fact that the shunt resistance can differ under forward and reverse bias [15]. The determined activation energy $E_{R,\mathrm{act}} \approx 0.55$ eV is close to half the silicon band gap; i.e., the temperature dependence of the depletion layer resistance is close to that of intrinsic semiconductor. This confirms the conclusion that a space-charge-limited current flows in this SC.

At $|V| > 4.5$ V, diode breakdown was observed. The detected increase in V_b with temperature (see table) is indicative of the avalanche breakdown mechanism in the studied structures.

3.2. Effect of Ultrasonic Loading

We emphasize that all the found AI changes in the parameters (Figs. 1–3, 4) were reversible; after USL termination, the SC parameters returned to the initial

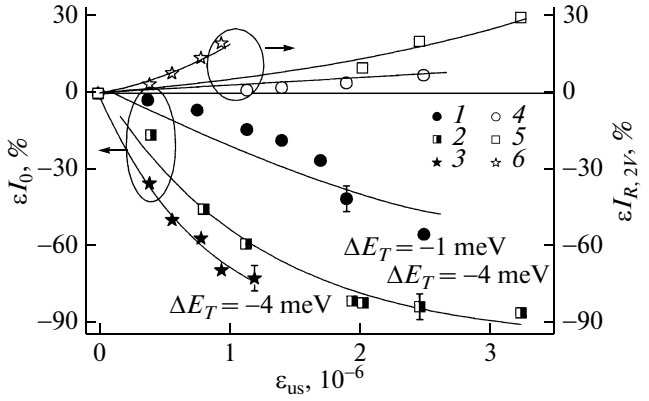

Fig. 1. Relative changes in the saturation current (*1–3*) and the reverse current at $V_R = 2$ V (*4–6*) under ultrasonic saturation; f_{us} = (*1*, *4*) 4.1, (*2*, *5*) 8.0, and (*3*, *6*) 26.1 MHz. The numbers near curves *1–3* are the maximum changes in the characteristic energy under ultrasonic saturation at a corresponding frequency.

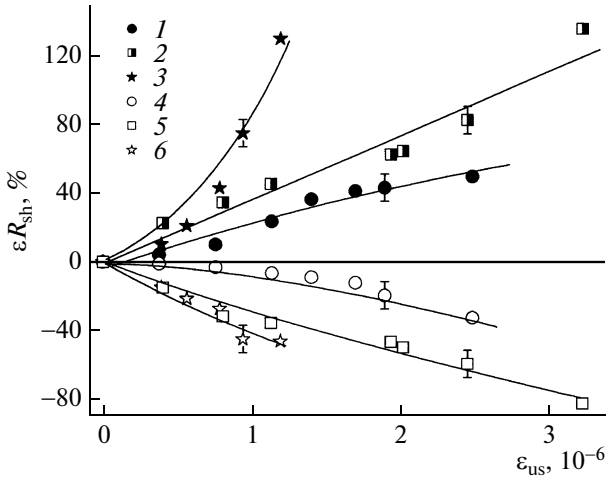

Fig. 2. Dependences of relative acoustically induced changes in the shunt resistance of the solar cell on the relative strain in the acoustic wave in dark (*1–3*) and upon exposure to light at λ = 900 nm (*4–6*); f_{us} = (*1*, *4*) 4.1, (*2*, *5*) 8.0, and (*3*, *6*) 26.1 MHz.

values for about 10 min. Let us consider these changes in more detail.

During USL, I_0 decreased quite significantly (Fig. 1), reaching 15–40% of the initial value. The amplitude dependence $I_0(\varepsilon_{us})$ at $\varepsilon_{us} > 10^{-6}$ exhibits flattening. The efficiency of AI changes increases with f_{us}. At the same time, the decrease ΔE_T is very small (Fig. 1) and is almost contained within the E_T determination error. Within the used model (formulas (3)–(5)), such behavior of $I_0(\varepsilon_{us})$ and $E_T(\varepsilon_{us})$ suggests that the defect parameters (r_d, δ_d) are constant during USL, with a simultaneous change in the number of deep level chains over which charge carriers are tunneled. Estimations using (5) show that the effective density ρ_d decreases by a factor of 3. In other words, AI ionization of defects arranged in the *p–n* junction region takes place. The AI ionization phenomenon was observed previously as well [16].

Figure 2 shows the AI changes in R_{sh}. We note that an increase in the efficiency of the ultrasound effect with f_{us} is also observed in this case. Furthermore, the effect is noteworthy of sample exposure to light on the R_{sh} behavior during USL; i.e., R_{sh} increases in dark by a factor of 1.5–2.5. In general, the appearance of R_{sh} is attributed to leakage currents over structural defects at the interface between *p*- and *n*-type regions [11, 17]. Hence, the increase in R_{sh}, as in the case of the ultrasound effect on I_0, can be explained by acoustic ionization of structural defects. Upon exposure to light at λ = 600 nm, the behavior of AI changes in R_{sh} is similar to the above and is not shown in Fig. 2. At the same time, the shunt resistance decreases during carrier photogeneration in the depth of the *p*-type region (λ = 900 nm). In our opinion, the prevalent AI effect in this case will be weakening recombination processes in the SC depth, which will be described below in more detail when considering the effect of USL on I_{sc}.

When light is mostly absorbed far from the *p–n* junction, I_{sc} can be estimated by the expression [17]

$$I_{sc} = W_{ph} e g S_s \frac{\lambda \alpha L_n (1 - R)}{hc(1 + \alpha L_n)}, \qquad (9)$$

where W_{ph} is the incident light intensity, R is the coefficient of reflection from the sample surface, g is the quantum yield coefficient, L_n is the diffusion length of electrons in the *p*-type region, and α is the light absorbance. The increase in I_{sc} (Fig. 3) observed under USL conditions is most likely caused precisely by the increase in L_n. The grounds for such a conclusion are as follows: first, it is believed [11] that L_n is controlling for I_{sc} in the case of such absorption; second, the diffusion length measurements we performed [10] showed that the increase in I_{sc} upon soundless heating correlates well with the change in the coefficient $\alpha L_n/(1 + \alpha L_n)$. We note that, although the change in I_{sc} is not very large (~10% at maximum ε_{us}), calculations show that a more than twofold increase in L_n should correspond to it.

It is known that one of the main recombination centers controlling L_n in Cz-Si:B is the $B_S O_{2i}$ impurity complex [18, 19]. Charge-dependent configuration bistability is inherent in this defect: it can be either in the $B_S O_{2i}^{sq}$ configuration (more probable for a positive singly charged state) or in $B_S O_{2i}^{st}$ (more probable in the neutral state). In our opinion, the $B_S O_{2i}^{sq} \longrightarrow B_S O_{2i}^{st}$ configuration transformation occurs during USL, which leads to their further transition to a neutral

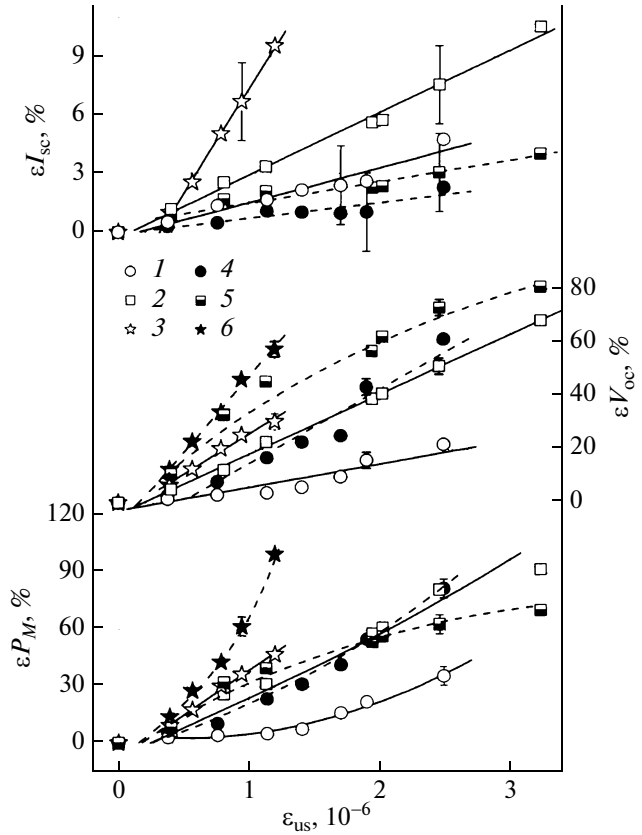

Fig. 3. Relative changes in the short-circuit current I_{sc}, open-circuit voltage V_{oc}, and maximum output power P_M as functions of the strain in the acoustic wave at $\lambda = 900$ nm (*1–3*) and $\lambda = 600$ nm (*4–6*); f_{us} = (*1*, *4*) 4.1, (*2*, *5*) 8.0, and (*3*, *6*) 26.1 MHz.

charge state. As a result, the B_SO_{2i} recombination activity decreases, which causes the observed increase in I_{sc}. We can see from the presented dependences that the efficiency of such a transformation almost linearly depends on ε_{us} and, hence, on the mechanical stress in the ultrasonic field. The increase in the efficiency of AI changes with the ultrasound frequency observed also in this case may be associated with the fact that the eigenfrequencies of impurity complex oscillations approach f_{us}. We note that metastability of defects is an important and positive factor for manifesting acoustodynamic effects in semiconductors [20]. Furthermore, the possibility of AI transformation of exactly the B_SO_{2i} complex is considered in [21].

When the sample is exposed to light at $\lambda = 600$ nm, carrier photogeneration in both *n*- and *p*-type regions, as well as in the *p–n* junction region, should be considered. Since $L_n\alpha \gg 1$ in this case, the photocurrent is almost independent of L_n. This leads to the absence of an increase in I_{sc} upon heating at $\varepsilon_{us} = 0$ (see table) and the much weaker, within measurement accuracy, effect of USL (Fig. 3). In our opinion, this weak effect

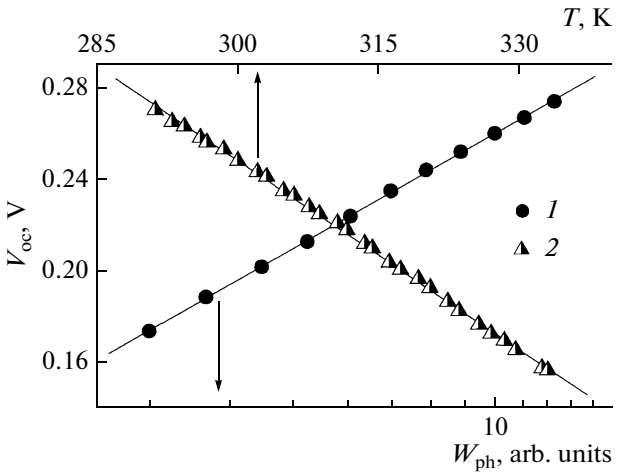

Fig. 4. Dependences of the open-circuit voltage V_{oc} of the solar cell on the incident light intensity (*1*) and temperature (*2*) at $\lambda = 900$ nm, $\varepsilon_{us} = 0$, and $T = 295$ K (*1*). Symbols are experimental data; lines are linear approximations.

is associated with a decrease in the surface recombination velocity due to AI ionization of surface levels.

The study of the dependences V_{oc} allowed not only more complete characterization of the effect of USL on the SC, but also was a certain confirmation of the charge transport mechanism proposed in Section 3.1. That is, setting $I = 0$ in (1a), for V_{oc}, we obtain

$$V_{oc} = \frac{E_T}{q}\ln\left[\frac{I_{sc}}{I_0} - \frac{V_{oc}}{I_0 R_{sh}} + 1\right]. \quad (10)$$

At $\lambda = 900$ nm, $I_{sc}/I_0 \gg V_{oc}//I_0R_{sh} > 1$ (see table); hence,

$$V_{oc} \approx (E_T/q)\ln[I_{sc}/I_0]. \quad (10a)$$

Using formula (9), the latter expression can be rewritten as

$$V_{oc} \approx \frac{E_T}{q}\left\{\ln W_{ph} + \ln\left[\frac{egS_s\lambda\alpha L_n(1-R)}{I_0 hc(1+\alpha L_n)}\right]\right\}. \quad (11)$$

Hence, the dependence of V_{oc} on the illumination intensity on the semilogarithmic scale should be linear. Exactly this is observed experimentally (Fig. 4). According to (11), the slope of this dependence is defined by the characteristic energy. The obtained value $E_T = 0.070$ eV is in complete agreement with the value determined by approximating the *I–V* characteristic (Section 3.1).

At the same time, it follows from expressions (10a), (2) and (5), (6) that, in the case of the validity of the tunneling charge transport mechanism, the temperature dependence of V_{oc} at $W_{ph} = \text{const}$ should be linear,

$$V_{oc}(T) = C_0 - C_1 T, \quad (12)$$

where the slope $C_1 = \chi E_T q^{-1}$ is defined by the product of the characteristic energy and the temperature coefficient of the increase in the saturation current through the diode, and the deviation of the zero term from the band gap at absolute zero $E_g(0)$ is defined by the concentration of levels through which tunneling occurs,

$$C_0 = q^{-1}[E_g(0) - E_T \ln(q\rho_d v_D S_s I_{sc}^{-1})]. \quad (13)$$

Formula (12) disregards the temperature dependence of I_{sc}, which, as experiments show (see table), is much weaker than that of V_{oc}.

Indeed, exactly the linear dependence $V_{oc}(T)$ (Fig. 4) was experimentally observed. Good agreement is observed for the slope of this dependence ($C_1 = 2.8 \times 10^{-3}$ V/K) and the parameters obtained from the analysis of the I–V characteristic shape ($\chi E_T q^{-1} = 3.4 \times 10^{-3}$ V/K) and the value of the zero term $C_0 = 1.07$ V and $E_g(0)/q = 1.21$ V for silicon. Thus, the luminance and temperature dependences of V_{oc} confirm the expediency of using the tunneling charge transport model.

The obtained data on the effect of USL on V_{oc} are shown in Fig. 3. The following should be noted.

(i) V_{oc} increases during USL, and this increase can reach 80%; in most cases, the dependences $\varepsilon V_{oc}(\varepsilon_{us})$ are close to linear.

(ii) AI changes are larger during carrier photogeneration near the p–n junction than in the case of light absorption in the diode base.

(iii) The efficiency of the acoustic effect increases with f_{us}; this is the feature also observed when considering other parameters. Taking into account (10), the mechanism of AI changes in V_{oc} should also be associated with ultrasonic ionization in the potential barrier region and the rearrangement of recombination centers.

Proceeding from the P_M definition, we can write

$$P_M = E_T I_m^2 q^{-1}[I_{sc} - I_m + I_0 + (E_T - qV_m)/(qR_{sh})]^{-1}, \quad (14)$$

where I_m and V_m are the current and voltage corresponding to the maximum output power. In fact, $I_m \approx 0.5 I_{sc}$ and $V_m \approx 0.5 V_{oc}$; hence

$$P_m \approx E_T I_{sc}^2 q^{-1}[2I_{sc} + 4I_0 + 2(2E_T - qV_{oc})/(qR_{sh})]^{-1}. \quad (15)$$

Thus, this quantity depends on the parameters, the mechanism of the AI effect on which was considered previously; hence, the P_M behavior under USL conditions can be foreseen. At the same time, since precisely P_M defines the SC efficiency, the experimentally observed effect of the significant (about twice) increase in the output power (Fig. 3) is promising for practical applications.

The reverse current also increases during USL (Fig. 1). Considering the current transmission mechanism (Section 3.1), this indicates an AI decrease in scattering by lattice vibrations and various defects,

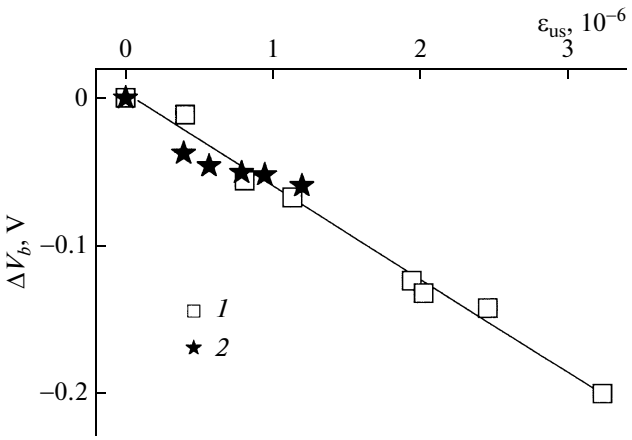

Fig. 5. Acoustically induced decrease in the breakdown voltage as a function of the strain in the acoustic wave; f_{us} = (*1*) 8.0 and (*2*) 26.1 MHz.

similarly to the ultrasound effect on I_{sc} at $\lambda = 900$ nm, considered above. One of the causes of this may be ordering of defect complexes in the ultrasonic field, i.e., the phenomenon described previously in [3]. The cause of AI changes in the breakdown voltage shown in Fig. 5 is similar: since the avalanche breakdown mechanism is inherent to the samples under study, the decrease in V_b indicates the increase in the carrier transit time between two sequential collisions (decrease in scattering). In contrast to all other parameters, changes in V_b are almost independent of f_{us}, which can indicate a decrease in lattice scattering unrelated to structural defects.

In general, the presented results show that ultrasonic waves represent a certain factor of ordering and synchronization of kinetic processes in solids, associated with both the transformation of the defect structure as a whole and charge transport in particular.

4. CONCLUSIONS

Based on the study of the temperature dependences of I–V characteristics of solar cells, the charge transport and photoelectric signal formation mechanisms were studied upon exposure to monochromatic light at various wavelengths.

The effect of USL on various parameters of a solar cell was experimentally studied in the dynamic mode for the first time. It was found that USL is accompanied by increases in the short-circuit current, open-circuit voltage, maximum output power, dark shunt resistance, and reverse current, as well as by a decrease in the saturation current through the diode and in breakdown voltage. The features of changes in these parameters were studied as functions of the ultrasound frequency and intensity.

Possible mechanisms of the acoustic effect on these parameters were analyzed. In particular, it was shown

that the observed effects can be accounted for by acoustically induced transformation of recombination centers (in particular, B_SO_{2i} complexes) and ionization of band-gap levels associated with various extended defects in the acoustic field.

The results of this study can be used for developing acoustically controlled photoconverters of various types.

REFERENCES

1. Ja. M. Olikh and O. Ya. Olikh, SEMST **1** (1), 19 (2004).
2. E. M. Zobov, M. E. Zobov, F. S. Gabibov, I. K. Kamilov, F. I. Manyakhin, and E. K. Naimi, Fiz. Tekh. Poluprovodn. **42**, 282 (2008) [Semiconductors **42**, 277 (2008)].
3. Ya. M. Olikh, N. D. Timochko, and A. P. Dolgolenko, Pis'ma Zh. Tekh. Fiz. **32** (13), 67 (2006) [Tech. Phys. Lett. **32**, 586 (2006)].
4. A. A. Podolyan and V. I. Khivrich, Pis'ma Zh. Tekh. Fiz. **31** (10), 11 (2005) [Tech. Phys. Lett. **31**, 408 (2005)].
5. A. Romanyuk, V. Spassov, and V. Melnik, J. Appl. Phys. **99**, 034314 (2006).
6. O. Ya. Olikh and T. N. Pinchuk, Pis'ma Zh. Tekh. Fiz. **32** (12), 22 (2006) [Tech. Phys. Lett. **32**, 517 (2006)].
7. A. Davletova and S. Zh. Karazhanov, J. Phys. D: Appl. Phys. **41**, 165107 (2008).
8. N. A. Guseinov, Ya. M. Olikh, and Sh. G. Askerov, Pis'ma Zh. Tekh. Fiz. **33** (1), 38 (2007) [Tech. Phys. Lett. **33**, 18 (2007)].
9. V. P. Melnik, Y. M. Olikh, V. G. Popov, B. M. Romanyuk, Y. V. Goltvyanskii, and A. A. Evtukh, Mater. Sci. Eng. B. **124–125**, 327 (2005).
10. O. Ya. Olikh, Ukr. Fiz. and Zh. **55**, 770 (2010).
11. A. Farenburkh and R. Bube *Fundamentals of Solar Cells: Photovoltaic Solar Energy Conversion* (Academic, New York, 1983; Energoatomizdat, Moscow, 1987).
12. V. V. Evstropov, Yu. V. Zhilyaev, M. Dumaeva, N. Nazarov, A. A. Sitnikova, and L. M. Fedorov, Fiz. Tekh. Poluprovodn. **34**, 1357 (2000) [Semiconductors **34**, 1305 (2000)].
13. S. V. Bulyarskii, Yu. V. Rud', L. N. Vostretsova, A. S. Kagarmanov, and O. A. Trifonov, Fiz. Tekh. Poluprovodn. **43**, 460 (2009) [Semiconductors **43**, 440 (2009)].
14. G. Lampert and P. Mark, *Injection Currents in Solids* (Academic, New York, 1970; Mir, Moscow, 1973).
15. A. A. Sherchenkov, B. G. Bugadyan, and A. V. Mazurov, Fiz. Tekh. Poluprovodn. **38**, 964 (2005) [Semiconductors **38**, 928 (2005)].
16. O. A. Korotchenkov and H. G. Grimmliss, Phys. Rev. B **52**, 14598 (1995).
17. S. M. Sze, *Physics of Semiconductors Devices* (Wiley Intersci., New York, 1981; Mir, Moscow, 1984), vol. 1.
18. J. Schmidt, K. Bothe, D. Macdonald, J. Adey, R. Jones, and D. W. Palmer, J. Mater. Res. **21** (1), 5 (2006).
19. J. Adey, R. Jones, D. W. Palmer, P. R. Briddon, and S. Oberg, Phys. Rev. Lett. **93**, 055504 (2004).
20. O. Ya. Olikh and I. V. Ostrovskii, Fiz. Tverd. Tela **44**, 1198 (2002) [Phys. Solid State **44**, 1249 (2002)].
21. O. Ya. Olikh, Fiz. Tekh. Poluprovodn. **43**, 774 (2009) [Semiconductors **43**, 745 (2009)].

Translated by A. Kazantsev